3-6-2019

Structural and magnetic properties of the CeCo5–CeZn5 solid solution and potential improvements upon iron substitution

Michael T. Onyszczak
Iowa State University and Ames Laboratory

Tej N. Lamichhane
Iowa State University and Ames Laboratory, tejl@iastate.edu

Sergey L. Bud'ko
Iowa State University and Ames Laboratory, budko@ameslab.gov

Paul C. Canfield
Iowa State University and Ames Laboratory, canfield@ameslab.gov

Structural and magnetic properties of the CeCo5–CeZn5 solid solution and potential improvements upon iron substitution

Abstract
In an effort to create high-performance permanent magnets with reduced critical rare earth content, we explored the CeCo5-xTx (T = transition metal or metalloid) family of compounds to investigate the effect of substitution on the material's magnetic properties. In our exploration of the CeCo5-xZnx system, we discovered a continuous solid solution at 900 degrees C between the CeCo5 and CeZn5 binary phases with ferromagnetism existing from the CeCo5 compound to the intermediate CeCo2.75Zn2.25 compound. Single crystal studies were also conducted revealing a relatively large anisotropy field of 11.5 T at 300 K for Ce0.96Ta0.04Co4.35Zn0.65. The addition of iron Ce0.79Ta0.07Co3.77Fe0.89Zn0.47 yielded further increases in Curie temperature and saturation magnetization to 800 K and 85.5 emu/g, respectively.

Keywords
Single crystal, Magnetization, Demagnetization factor, Arrott plot, Transition temperature, Anisotropy constant

Disciplines
Materials Science and Engineering | Metallurgy

Structural and magnetic properties of the $CeCo_5$–$CeZn_5$ solid solution and potential improvements upon iron substitution

Michael T. Onyszczak[a,b], Tej N. Lamichhane[a,b], Sergey L. Bud'ko[a,b], Paul C. Canfield[a,b], Andriy Palasyuk[b,□]

[a] *Department of Physics and Astronomy, Iowa State University, Ames, IA 50011, USA*
[b] *Ames Laboratory, Iowa State University, Ames, IA 50011, USA*

ARTICLE INFO

Keywords:
Single crystal
Magnetization
Demagnetization factor
Arrott plot
Transition temperature
Anisotropy constant

ABSTRACT

In an effort to create high-performance permanent magnets with reduced critical rare earth content, we explored the $CeCo_{5-x}T_x$ (T = transition metal or metalloid) family of compounds to investigate the effect of substitution on the material's magnetic properties. In our exploration of the $CeCo_{5-x}Zn_x$ system, we discovered a continuous solid solution at 900 °C between the $CeCo_5$ and $CeZn_5$ binary phases with ferromagnetism existing from the $CeCo_5$ compound to the intermediate $CeCo_{2.75}Zn_{2.25}$ compound. Single crystal studies were also conducted re- vealing a relatively large anisotropy field of 11.5 T at 300 K for $Ce_{0.96}Ta_{0.04}Co_{4.35}Zn_{0.65}$. The addition of iron $Ce_{0.79}Ta_{0.07}Co_{3.77}Fe_{0.89}Zn_{0.47}$ yielded further increases in Curie temperature and saturation magnetization to 800 K and 85.5 emu/g, respectively.

1. Introduction

Since their discovery in the 1960's, rare-earth cobalt, RCo_5 (R = Rare-earth metal), alloys have been the subject of significant re- search due to their intrinsic magnetic properties which are suitable for industrial, high-temperature permanent magnets [1,2]. However, only $SmCo_5$ magnets have been commercially produced due to the other RCo_5 alloys lacking the critical combination of a sufficiently large uniaxial anisotropy and an adequately high Curie temperature.

The use of Ce in RCo_5 magnets has been of recent interest due to the relative abundance of Ce in comparison to the other, more critical, rare-earth elements. $CeCo_5$ has a smaller saturated magnetic moment and decreased Curie temperature as compared to YCo_5, $PrCo_5$, and $SmCo_5$, its anisotropy constant is smaller than $SmCo_5$, 7.2 MJ/m^3 versus 11.2 MJ/m^3 at room temperature [3,4]. Despite its diminished mag- netic properties, $CeCo_5$ holds the potential to be a so-called 'gap magnet'. The need for gap magnets arises from the 'gap' in magnetic energy densities, $(BH)_{max}$, between high-performance magnets, such as $SmCo_5$ and $Nd_2Fe_{14}B$, and lower-performance, lower cost magnets, such as Alnico and ferrites. Quantitatively, a gap magnet would have $(BH)_{max}$ in the range of 10–20 MGOe which would fill the gap in energy pro- ducts between the currently known high and low-performance magnets.

As part of our ongoing work to identify candidates to fulfill this need for a gap magnet, we have studied the Ce–Co–T (T = Ni, Cu, Zn) systems to search for new candidates for magnetic materials and also to characterize the intrinsic magnetic properties of these materials. The Ce–Co–Zn system was of particular interest since there has only been limited investigation of the system, and the existing work was limited to low temperature (470 K) studies of the phase equilibria with no mag- netic characterization [5,6]. This previous work revealed a limited solid solution where compositions close to $CeCo_{2.6}Zn_{2.4}$ form with the $CaCu_5$-type structure, but there were no reports of continuous solubility be- tween $CeCo_5$ and $CeZn_5$. However, investigations of the Ce–Ni–Zn system revealed that at higher temperatures (800 °C) the $Ce(Ni,Zn)_5$ compound forms a continuous solid solution between $CeNi_5$ and $CeZn_5$ [7]. This fragmentation of the solid solution at lower temperatures is likely due the instability of $CeCo_5$ which decomposes into Ce_2Co_{17} and Ce_5Co_{19} at 600 °C [8]. The similarities between the Ce–Ni–Zn and Ce–Co–Zn systems led us to characterize the $Ce(Co,Zn)_5$ system at a higher temperature and to investigate the role of Zn in this compound's intrinsic properties.

Here we report the successful synthesis of polycrystalline samples of $Ce(Co,Zn)_5$ across the entire solid solution followed by characterization of their structural and magnetic properties. We study the significant coercivity that appears in the as-grown polycrystalline samples. This coercivity appears without any defects or secondary phases apparent in the microstructure of the materials (within SEM resolution limits). We also report the synthesis of single crystal samples of the approximate

composition $Ce_{0.96}Ta_{0.04}Co_{4.35}Zn_{0.65}$ and $Ce_{0.79}Ta_{0.07}Co_{3.77}Fe_{0.89}Zn_{0.47}$ (grown out of Ta crucibles, containing small amounts of Ta impurities) and the characterization of their structural and magnetic properties.

2. Experimental procedures

2.1. Synthesis

Polycrystalline samples were synthesized by placing a stoichiometric mixture of high purity elements (Ce (99.99%) from Ames Laboratory MPC, Cu (99.999%) from Puratronic, Zn (99.999%), and Co (99.95%) from Alfa Aesar) in an alumina crucible. The crucible was sealed in a fused silica ampoule under a partial pressure Ar atmosphere to protect against oxidation at high temperatures. The ampoule was then placed in a box furnace and heated to 450 °C over two hours and held at that temperature for ten hours to encourage the Zn to melt and form com- pounds with lower vapor pressures. The temperature was then increased to 950 °C over two hours and again held for ten hours to help reduce possible problems associated with Zn vapor pressure. The furnace tem- perature was then increased to 1200 °C over two hours and held for two more hours to ensure all materials had melted and combined. The fur- nace was cooled to 900 °C over 30 min to solidify the alloy. The material was then held at 900 °C for 50 h to anneal. Finally, the ampoule was removed from the furnace and quenched into ice water. No significant signs of Zn vaporization or loss were observed in any of the samples.

The single crystal samples were produced via the self-flux solution growth method [9,10]. The constituent elements (Ce (99.99%) from Ames Laboratory MPC, Cu (99.999%) from Puratronic, Zn (99.999%, Fe (99.99%), and Co (99.95%) from Alfa Aesar) were combined with in- itial compositions of $Ce_{18}Co_{55.8}Fe_{9.8}Zn_{16.4}$ and $Ce_{18}Co_{65.6}Zn_{16.4}$, placed into a 3-capped Ta crucible [11], and welded under an Ar atmosphere. The Ta container was then sealed in a fused silica ampoule under a partial pressure Ar atmosphere before being placed into a box furnace. The ampoule was heated to 900 °C in four hours and held at that temperature for three hours to allow the liquid Ce and Zn to mix and react with the other elements to minimize the effect of Zn vapor pres- sure. Then, the temperature was increased to 1200 °C over three hours and held there for ten hours to allowing the entire sample to melt and homogenize. The sample was cooled at a rate of 1.5 °C/h to its final temperature of 1070 °C where the sample was removed from the fur- nace and decanted via centrifuge. This process produced $\sim 1 \times 1 \times 0.1\ cm^3$ plates.

Attempts were made to replicate the heat treatment performed on the $Ce(Co,Cu)_5$ system [12], but the results produced no significant or consistent effects on magnetic properties. Furthermore, due to the low boiling point of Zn, there was significant decomposition of the samples as Zn readily vaporized and caused uncontrolled decomposition in several attempts.

2.2. X-ray characterization

The crystal structure of the polycrystalline $CeCo_{5-x}Zn_x$ samples and the single crystalline Fe-doped sample were determined via powder X- ray diffraction (XRD) using a Rigaku Miniflex II diffractometer with a Cu tube and monochromator. Data were collected in a 2θ range of 5–100 degrees in 0.02-degree steps and a 2s collection time. The structural refinement was performed using the full-profile Rietveld method within the FullProf program package [13].

Single-crystal diffraction data were collected at room temperature using a Brucker SMART APEX II diffractometer (Mo K_α-radiation) equipped with a CCD area detector. Five sets of 360 frames with 0.5° scans in ω and exposure times of 10–15 s per frame were collected. The reflection intensities were integrated using the SAINT subprogram in the SMART software package [14]. The space group was determined using the XPREP program and the SHELXTL 6.1 software package [15]. Empirical absorption corrections were made using the SADABS program [16]. Finally, each structure was solved by direct methods using SHELXTL 6.1 and refined by full-matrix least-squares on F_0^2, with anisotropic thermal parameters and a secondary extinction parameter. Crystallographic data are presented in tables in Appendix A.1.

2.3. Magnetic characterization

Magnetic properties (temperature dependent and field dependent magnetization) were measured using a Quantum Design, 3 Tesla, Vibrating Sample Magnetometer (VSM) in the standard option for measurements between 50 K and 400 K and using the oven option for measurements between 300 K and 1000 K. A Quantum Design MPMS was used to characterize the magnetic properties from 2 K to 300 K. Samples selected for measurements were small, ~5 mg, samples that were fractured along {0001} planes and were measured with the field roughly parallel to the [0001] direction, crystallographic *c* axis.

The single crystalline material was characterized using a Quantum Design MPMS to characterize its Curie temperature, saturation magnetization, and anisotropy constants. A thin plate was selected and then polished into a square geometry. The plate was measured with the applied field both parallel and perpendicular to its *c* axis.

2.4. Scanning electron microscopy (SEM) & energy-dispersive X-ray spectroscopy (EDS) characterization

Samples for metallographic examination were embedded in 1-inch diameter epoxy resin pucks and polished with various grits of silicon carbide followed by a glycol-based, polycrystalline diamond suspension. Imaging studies of the samples were performed on an FEI Teneo field emission scanning electron microscope. Their compositions were determined via energy dispersive X-ray spectra obtained using an Oxford EDS/EBSD module averaging over 3–5 regions on their metallographically prepared surfaces. Some results of these studies are shown in Figs. A.11 through A.15 of the appendix.

3. Structure and composition analysis

3.1. SEM/EDS examination and composition analysis

SEM backscattered electron images of the as-grown polycrystalline samples (see appendix) show a uniformity in composition across the EDS analyzed regions with minor exceptions of several topographical defects (scratches and pitting) which suggests a uniform composition throughout the sample. EDS compositional analysis determined the Ce content of most of these samples to be between 16.5 and 16.8 atomic percent which is close to the predicted 16.67 atomic percent Ce in a $CaCu_5$-type structure.

EDS elemental analysis confirmed the actual Zn concentration in the polycrystalline samples to be very close to their nominal Zn concentration, therefore we will refer to samples by their nominal Zn concentration.

Additionally, SEM/EDS analyses of the single crystal samples determined their stoichiometries to be $Ce_{0.96}Ta_{0.04}Co_{4.35}Zn_{0.65}$ and $Ce_{0.79}Ta_{0.07}Co_{3.77}Fe_{0.89}Zn_{0.47}$ for the un-doped and Fe-doped single crystalline samples respectively. The appearance of Ta in the samples is best explained by the partial dissolution of the Ta containers that the crystals were grown in. SEM imaging of the single crystalline samples illustrates the single phase nature of the samples despite the uptake of Ta from the growth crucible. The under-occupancy of Ce suggests a deviation from the $CaCu_5$ structure to a $TbCu_7$ structure which allows for a substitution of Ce on the *a* site with a transition metal "dumbbells" on the *2e* sites. In both cases Ta appears to occupy the *2e* sites. However in case of the Fe-doped sample a mixture of Co, Fe, Zn, and Ta must occupy the *2e* sites to match the EDS composition. The appearance of various transition metal dumbbells such as Ta, Co, and Zn have previously been reported to occupy the *2e* site in similar systems [12,17,18].

3.2. X-ray analysis and crystal structure determination

Powder X-ray diffraction analyses were performed on crushed and powdered as-grown samples with varying Zn concentrations. The smooth shifting of the Bragg peaks with the addition of Zn (as seen in Fig. 1) strongly suggests the existence of a solid solution between $CeCo_5$ and $CeZn_5$ at 900 °C. The linear relationship between lattice parameters and Zn concentration (as seen in Fig. 2) further supports the existence of a continuous solid solution. Fig. 3 shows a typical fit of a powder diffraction pattern of a polycrystalline sample and demonstrates the single phase nature of the sample.

A single crystal was picked up from a polycrystalline sample with Zn = 2.5 and its crystal structure was evaluated using single crystal refinement method. However, refinements using a $CaCu_5$ model re- sulted in large electronic residuals as seen in Fig. 4(c). If the crystal was refined using $TbCu_7$-type structure, a significant improvement in the

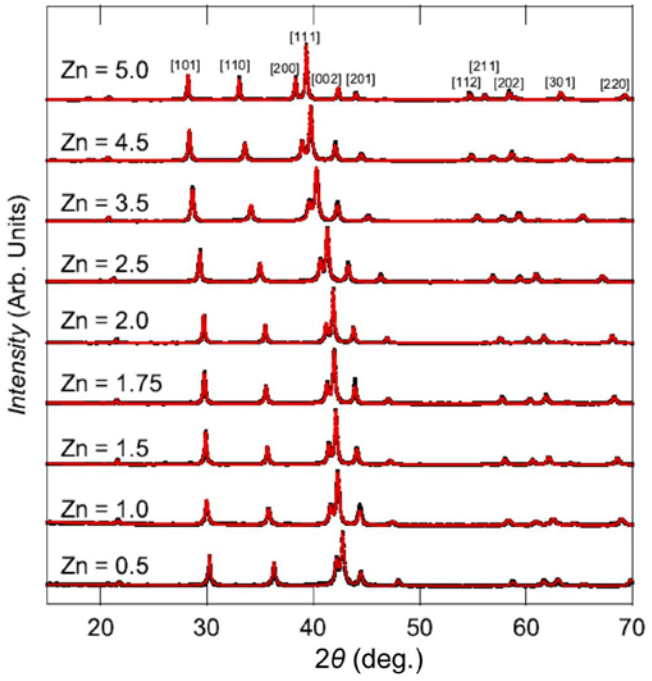

Fig. 1. Diffraction data for various Zn concentrations. Observed values in black, $CeCo_{5-x}Zn_x$ refined fits in red. No additional peaks are observed other than the $CaCu_5$/$TbCu_7$ type peaks. Higher Zn concentrations offset vertically for readability.

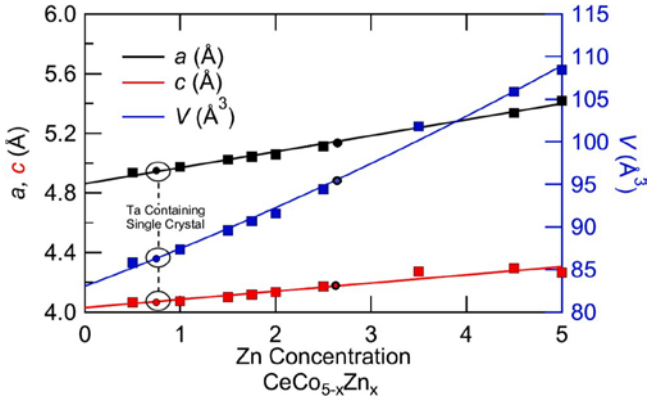

Fig. 2. Refined lattice parameters of $CeCo_{5-x}Zn_x$ with linear fits for lattice parameters and cubic fit for unit cell volume. Circular markers denote single crystal refinements and square markers denote powder refinements.

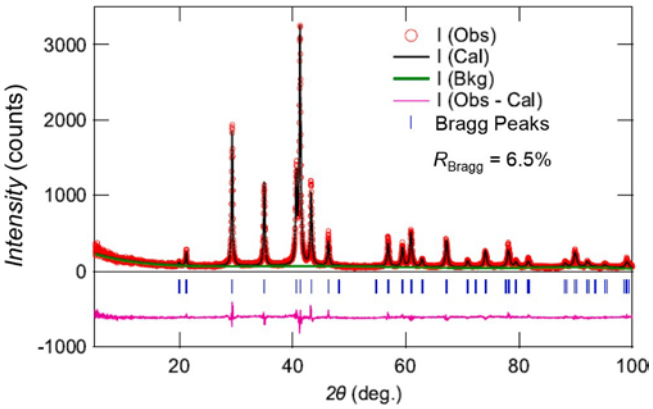

Fig. 3. A typical example of a predominantly single-phase polycrystalline XRD pattern for a Zn = 2 sample. *I* (Obs), *I* (Cal), and *I* (Bkg) are the experimental, Rietveld refined, and instrumental background data, respectively. The lower portion of the graph shows the Bragg's-peak positions with blue vertical lines and the differential X-ray diffractogram *I* (Obs-Cal) in pink.

residual electron density was observed when Zn–Zn dumbbells were incorporated. The occupancy of the *2e* site in this specific sample was 4–5% which suggests some deviation from the $CaCu_5$-type structure. In this specific case also the EDS confirmed larger Ce deficiency (see Fig. A.11). However, according to our SEM/EDS evaluation of other poly- crystalline samples (Figs. A.13, A.14), this deviation is even smaller and estimated 2*e* occupancy in general may well fit within 1–2%.

Single crystal refinement of the single crystalline sample $Ce_{0.96}Ta_{0.04}Co_{4.35}Zn_{0.65}$ revealed that the Ta presence is best described as partial Ce substitution by Ta–Ta dumbbells, i.e., each Ce in 1*a* is replaced Ta–Ta pair in the *2e* crystallographic site. The unintended incorporation of Ta is a common issue in single crystal growths of the CeT_5 type compounds due to the dissolution of the Ta crucible, but Ta is believed to have a negligible influence on any properties as compared to a Ta-free sample [12]. Specific details of these single crystal refinements are found in the appendix.

The Fe-doped single crystalline sample $Ce_{0.79}Ta_{0.07}Co_{3.77}Fe_{0.89}Zn_{0.47}$ was unable to be characterized using the single crystal X-ray techniques due to significant surface texturing, and crystal intergrowths. This made it difficult to selecting a piece with uniform and well-defined edges. Instead, the sample was analyzed using powder diffraction. Qualitatively, the X-ray patterns of $Ce_{0.79}Ta_{0.07}Co_{3.77}Fe_{0.89}Zn_{0.47}$ (Fig. A.16 in appendix) was very similar to typical $CaCu_5$-type patterns observed in this system (Fig. 1). However, considering the EDS analysis, which estimated Ce content to be 13.2 instead of 16.7 at.% (Fig. A.16), the 1D structural channels must be filled with Ce/T (T = Ta, Co, Fe, Zn) mixtures instead of single Ce atoms, in a way that was described above. Nevertheless the exact occupations of those atomic mixtures remain unknown due to ambiguity of present powder diffraction analysis. Herein we used simple substitution of Ce by pairs of Ta–Ta atoms. It partially describes present atomic disorder, but misses subtleties of the exact content of the dumbbells, etc.

Polycrystalline powder X-ray diffraction results were analyzed using both $CaCu_5$ and $TbCu_7$-type models, but the relative differences in lat- tice parameters and the profile residual (R_p) were negligible. A slight improvement in the Bragg peak residuals (R_{Bragg}) were observed in the $TbCu_7$ model, but this difference could be attributed to the increase in the number of model parameters as compared to the $CaCu_5$ model. This strongly suggests that this solid solution is best described as a $CaCu_5$- type structure with a minimal amount of disorder.

4. Magnetic properties

The Curie temperatures (T_C) of various Zn concentrations were estimated by examining the point of maximum slope in the temperature

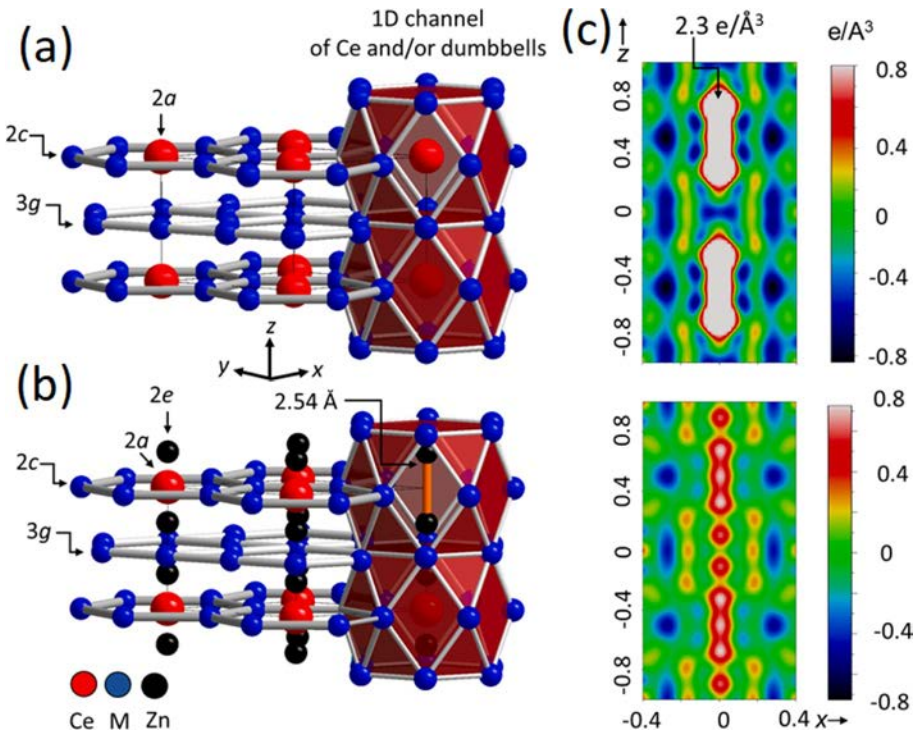

Fig. 4. Single crystal refinement of $Ce_{0.96}Co_{2.38}Zn_{2.65}$ [110] views of (a) $CaCu_5$-type and (b) $TbCu_7$-type structures with and without Zn "dumbbells", respectively and (c) difference electron density maps of structural solutions without "dumb-bells" (upper) showing significant residual electron density peaks in 1D structural channels at (0 0 z), $z \approx 0.3$, and with "dumb-bells" (lower) showing a decrease in the residual electron density peaks.

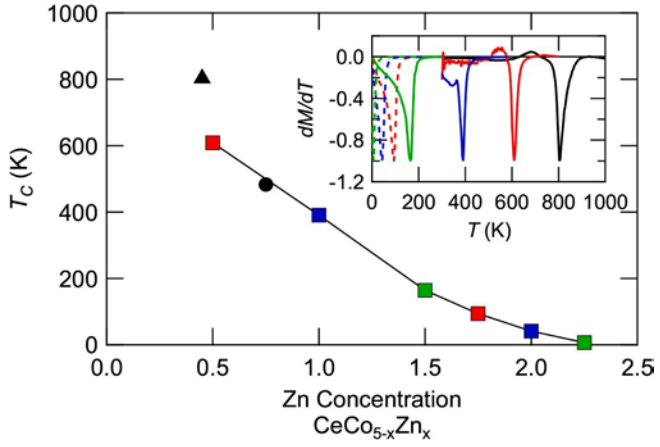

Fig. 5. Curie temperatures of various Zn concentrations with black triangular marker indicating the Fe-doped sample and black circular marker indicates T_C as determined from the Arrott plot of the single crystalline sample. The inset shows the temperature derivatives of (normalized) magnetic moment which were used to determine the Curie temperature of the other samples. Magnetic field of 0.01 T was used during the magnetization data collection.

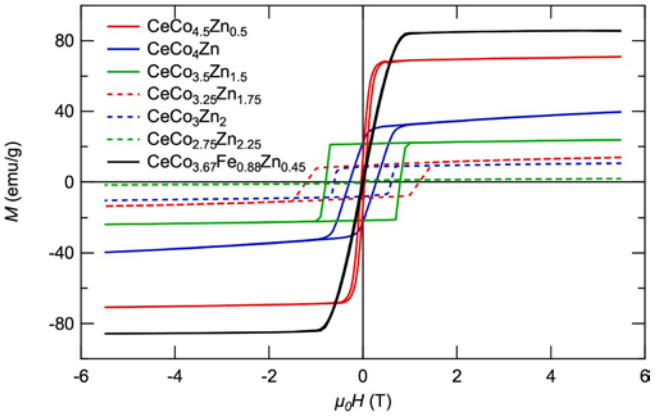

Fig. 6. Plot of magnetization loops at 5 K for various ferromagnetic compositions of $CeCo_{5-x}Zn_x$ roughly aligned with c-axis parallel to the applied magnetic field.

dependent magnetization curves (Fig. 5 inset), and thus inferred T_C, as a function of Zn concentration, is shown in Fig. 5. The saturated moment (M_{sat}) and the magnetic coercivity (H_C) of the various compounds were characterized at 5 K and are shown in Figs. 6 and 7. M_{sat} was determined to by taking the value of magnetization at 5.5 T, and H_C was determined by taking the average field needed to achieve zero magnetization when either decreasing or increasing the applied field.

A monotonic decrease of M_{sat} is induced by substituting magnetic Co for non-magnetic Zn. On the other hand, a conspicuous maxima in H_C near $CeCo_{3.25}Zn_{1.75}$ is found; this cannot be attributed to the typical coercivity mechanisms of spinodal decomposition, formation of a secondary pinning-phase, or other types of matrix decomposition since these structural features would appear in its SEM image (Fig. A.14 in the appendix), but are clearly absent. Even examinations at the SEM resolution limits did not reveal those features. Besides, coercivity is detected in the as-cast samples, without any hardening heat treatment applied. The high resolution TEM experiments to elucidate the coercivity mechanism are underway. The decrease in H_C beyond $CeCo_{3.25}Zn_{1.75}$ can be explained as the material approaching a ferromagnetic – paramagnetic transition near $CeCo_{2.5}Zn_{2.5}$ which forces H_C to zero by definition.

To provide comparison to the polycrystalline samples and to determine anisotropic properties, M_{sat}, T_C, H_C, and magnetocrystalline anisotropy energy densities were measured using the $Ce_{0.96}Ta_{0.04}Co_{4.35}Zn_{0.65}$ single crystal sample. This sample has T_C, M_{sat}, and H_C values consistent with the trend exhibited in other Zn substituted samples (Figs. 5 and 7).

The Curie temperature of $Ce_{0.96}Ta_{0.04}Co_{4.35}Zn_{0.65}$ single crystalline

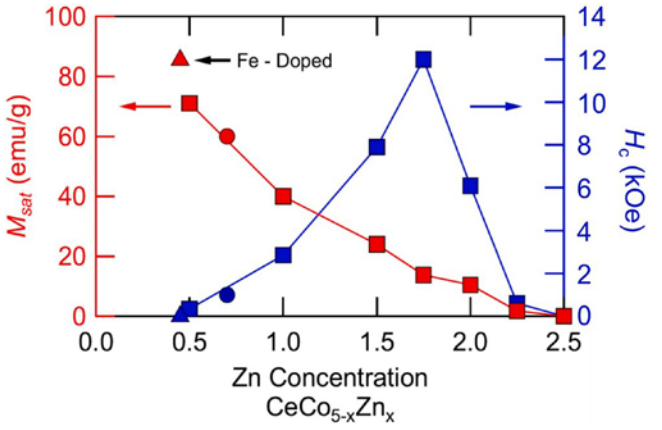

Fig. 7. Dependence of coercivity () and saturation magnetization (M_{sat}) on Zn concentration at 5 K. Triangular marker denotes Fe-doped composition, and circular marker denotes data from the un-doped single crystal sample.

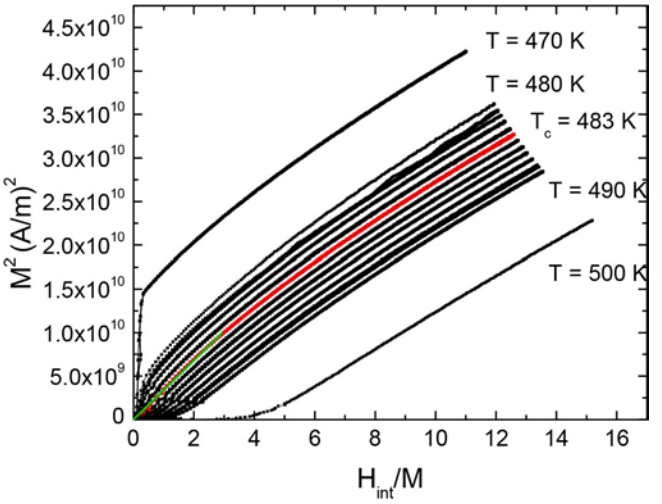

Fig. 8. Arrot plot for the single crystalline sample $Ce_{0.96}Ta_{0.04}Co_{4.35}Zn_{0.65}$ with various isotherms. The Curie temperature of 483 K is inferred from the corresponding isotherm being nearly linear and passing through the origin.

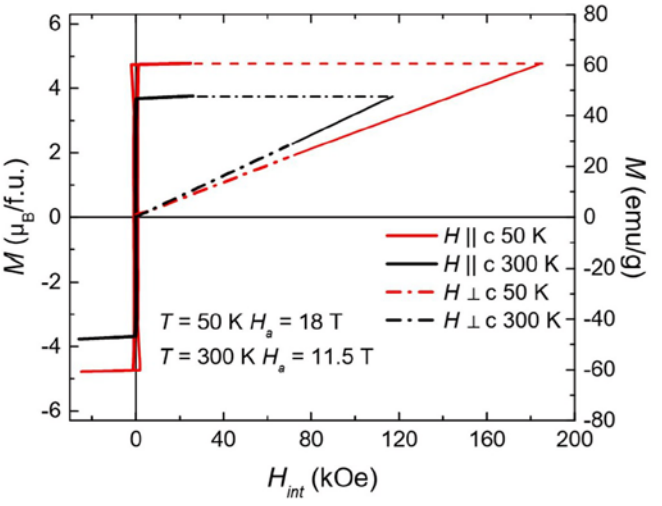

Fig. 9. Easy and hard axis magnetization at 50 K and 300 K for $Ce_{0.96}Ta_{0.04}Co_{4.35}Zn_{0.65}$.

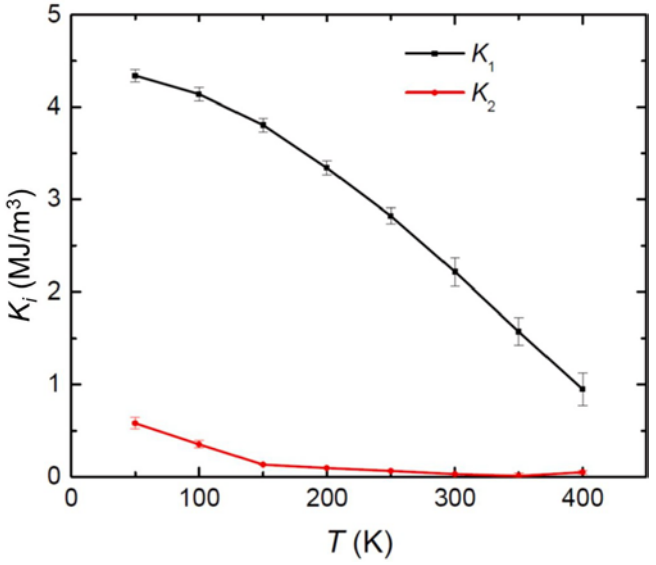

Fig. 10. Temperature dependent magnetocrystalline anisotropy density of single crystalline $Ce_{0.96}Ta_{0.04}Co_{4.35}Zn_{0.65}$.

sample was determined via the Arrott plot method (Fig. 8). Isotherms were taken between 480 K and 490 K every 1 K, and T_C was estimated to be 483 K. The isotherm plots exhibit some curvature, which calls for more sophisticated analysis to obtain the generalized Arrott plot [19–21]. However, in our case this might be difficult because of sample degradation at $T > 550$ K. Even our analysis gives T_C within 2–4 K.

Easy axis and hard axis magnetization measurements at 50 K and 300 K (Fig. 9) determined H_C to be 18 T and 11.5 T, respectively.

The temperature dependent magnetocrystalline anisotropy energy density was determined using the Sucksmith-Thompson method [22–24] by using the hard axis magnetization isotherms from 50 K to 400 K (Fig. 10).

5. Conclusions

A continuous solid solution between $CeCo_5$ and $CeZn_5$ at 900 °C is observed and is best described as a $CaCu_5$-type structure with a minimal amount of disorder on the *2e* crystallographic sites as demonstrated by the single phase nature of its SEM images, the smooth, continuous shifts observed in X-ray diffraction peaks, and the single crystal refinement which is best fit with a $CaCu_5$-type structure with small disorder, i.e., presence of dumbbell *2e* sites.

The magnetic properties of the solid solution show a significant increase coercivity with the addition of Zn with a clear maximum near $CeCo_{3.25}Zn_{1.75}$, but a monotonic decrease in the saturated moment was observed as Co is removed. The origin of the large coercivities observed in the as-grown crystals currently is unexplained as EDS and X-ray diffraction showed no such precipitates or obvious structural me- chanism which could create this coercivity.

The addition of Fe remains a viable method to improve magnetic properties such as Curie temperature and saturated moment. The sample doped with Fe showed significant improvements to Curie tem- peratures and saturated moment for its respective Zn concentration.

Acknowledgments

This research was supported by the Critical Materials Institute, an Energy Innovation Hub funded by the U.S. Department of Energy, Office of Energy Efficiency and Renewable Energy, Advanced Manufacturing Office. This work was performed at the Ames Laboratory, operated for DOE by Iowa State University under Contract No. DE-AC02-07CH11358.

Appendix A. SEM/EDS data & crystallographic data

Figs. A.11, A.12, A.13, A.14, A.15, A.16.
Tables A.1, A.2, A.3, A.4, A.5.

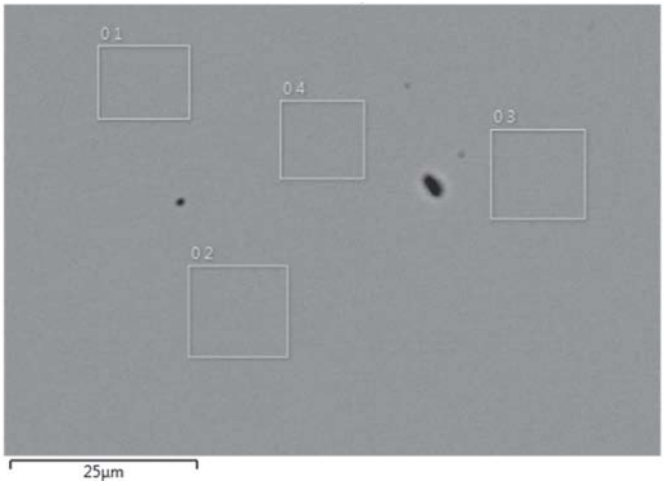

Label	Ce	Co	Zn
1	15.9	39.9	44.2
2	16.1	39.7	44.2
3	16.1	39.6	44.3
4	16.0	39.5	44.5
Avg.	16.0	39.7	44.3
Std. Dev.	0.1	0.2	0.1

Fig. A.11. SEM backscattered electron images of $Ce_{0.96}Co_{2.38}Zn_{2.65}$, with elemental analysis of each scan region.

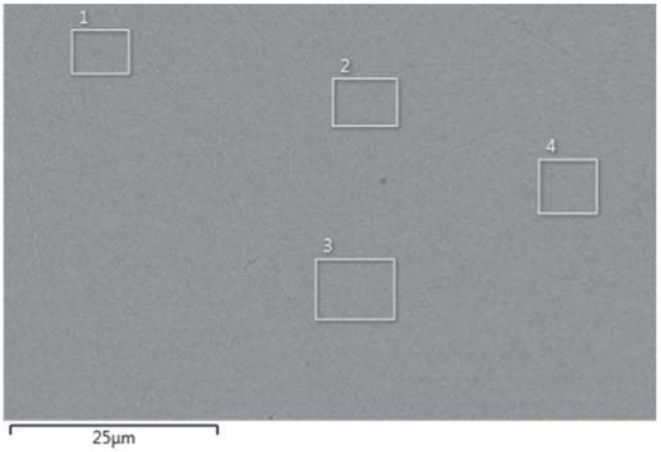

Label	Ce	Ta	Co	Zn
1	15.8	0.6	72.5	11.1
2	15.7	0.6	72.8	10.9
3	15.8	0.6	72.7	10.9
4	15.7	0.6	72.5	11.2
Avg.	15.8	0.6	72.6	11.0
Std. Dev.	0.05	0.02	0.1	0.1

Fig. A.12. SEM backscattered electron images of $Ce_{0.96}Ta_{0.04}Co_{4.35}Zn_{0.65}$, with elemental analysis of each scan region.

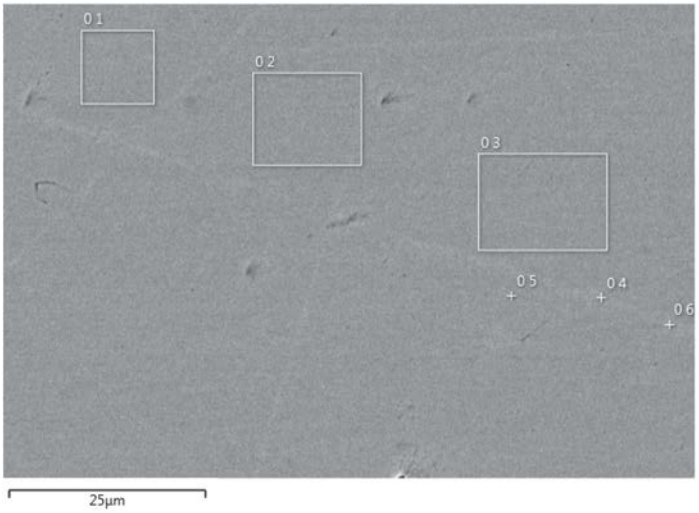

Label	Ce	Co	Zn
1	16.7	54.2	29.1
2	16.6	54.2	29.2
3	16.7	54.1	29.2
4	16.8	54.2	29.0
5	16.6	54.3	29.1
6	16.7	54.3	29.0
Avg.	16.7	54.2	29.1
Std. Dev.	0.07	0.07	0.08

Fig. A.13. SEM backscattered electron images of $CeCo_{3.25}Zn_{1.75}$, with elemental analysis of each scan region.

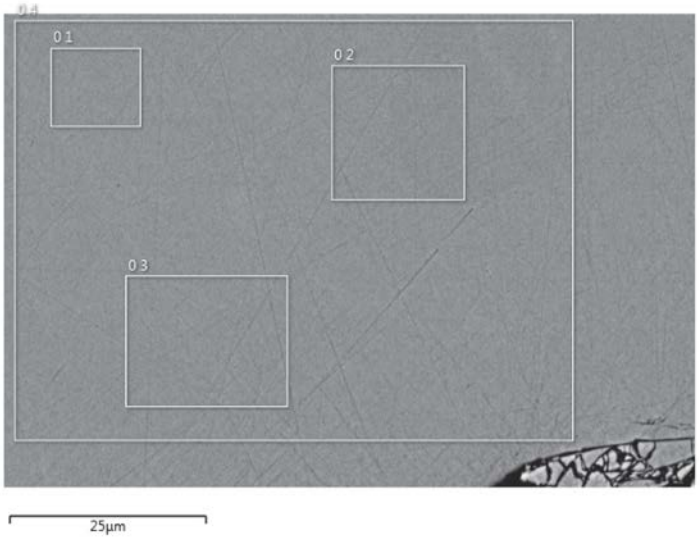

Label	Ce	Co	Zn
1	16.7	50.8	32.5
2	16.7	50.8	32.5
3	16.7	50.9	32.4
4	16.7	50.8	32.5
Avg.	16.7	50.8	32.5
Std. Dev.	0.01	0.02	0.02

Fig. A.14. SEM backscattered electron images of $CeCo_3Zn_2$, with elemental analysis of each scan region.

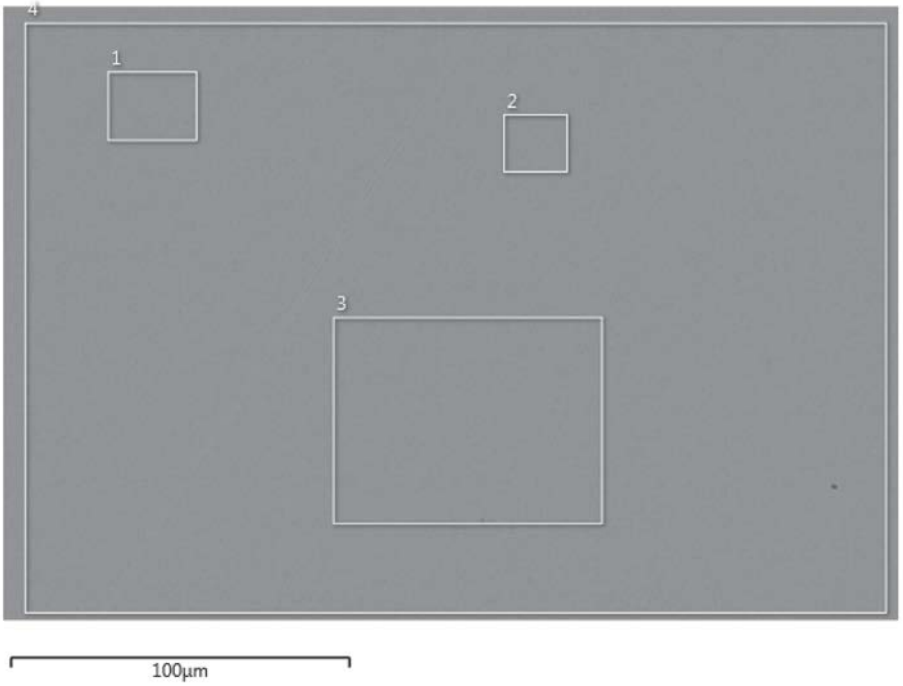

Label	Ce	Ta	Co	Fe	Zn
1	13.1	1.2	62.9	15.0	7.8
2	13.0	1.2	62.7	15.1	8.0
3	13.2	1.2	63.2	14.7	7.7
4	13.3	1.3	62.7	14.9	7.8
Avg.	13.2	1.2	62.9	14.9	7.8
Std. Dev.	0.1	0.04	0.2	0.1	0.09

Fig. A.15. SEM backscattered electron images of $Ce_{0.79}Ta_{0.07}Co_{3.77}Fe_{0.89}Zn_{0.47}$, with elemental analysis of each scan region.

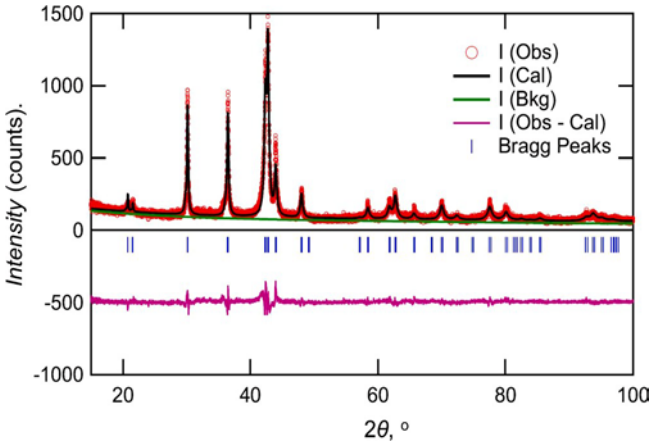

Fig. A.16. Powder XRD pattern from the crushed Fe-doped single crystalline sample $Ce_{0.79}Ta_{0.07}Co_{3.77}Fe_{0.89}Zn_{0.47}$. *I* (Obs), *I* (Cal), and *I* (Bkg) are the experimental, Rietveld refined, and instrumental background data, respectively. The lower portion of the graph shows the Bragg's-peak positions with blue vertical lines and the differential X-ray diffractogram *I* (Obs-Cal) in pink.

Table A.1
Powder X-ray data and refinement parameters for Fe-doped sample $Ce_{0.79}Ta_{0.07}Co_{3.77}Fe_{0.89}Zn_{0.47}$.

EDS composition	$Ce_{0.79}Ta_{0.07}Co_{3.77}Fe_{0.89}Zn_{0.47}$
Refined composition	$Ce_{0.93}Ta_{0.14}Co_{3.69}Fe_{0.86}Zn_{0.45}$
Space group, *Z*	*P*6/ , 1
Unit cell (Å),	4.918(1)
	4.108(1)
$\mathcal{V}$ (Å^3)	86.04(2)
Radiation	Cu κ_α
2θ range	5.0–100.0 deg.
No. of data collected	9.495 data points
No. of unique data	41 Bragg reflections
No. of variables	17
Residuals, $\Re_p/\Re_{Bragg}$, %	10.2/8.7

Table A.2
Atomic coordinates, equivalent isotropic displacement parameters (Å$^2 \times 10^3$) and site occupancies refined for Fe-doped sample $Ce_{0.79}Ta_{0.07}Co_{3.77}Fe_{0.89}Zn_{0.47}$. Occupancies and displacement parameters for 2c and 3g sites were fixed.

Element	Wickoff Site	Occupancy		*y*	*z*	*U* (*eq*)
Ce	1a	0.93(1)	0	0	0	13(1)
Ta	2e	0.07(1)	0	0	0.360(4)	13(1)
Co	3g	0.73	1/2	0	1/2	15
Fe	3g	0.17	1/2	0	1/2	15
Zn	3g	0.10	1/2	0	1/2	15
Co	2c	0.73	1/3	2/3	0	10
Fe	2c	0.17	1/3	2/3	0	10
Zn	2c	0.10	1/3	2/3	0	10

Table A.3
Single crystal and refinement data for Ta-free $Ce_{0.96}Co_{2.38}Zn_{2.65}$ and Ta-doped $Ce_{0.96}Ta_{0.04}Co_{4.35}Zn_{0.65}$.

EDS composition	$Ce_{0.96}Co_{2.38}Zn_{2.65}$	$Ce_{0.96}Ta_{0.04}Co_{4.35}Zn_{0.65}$
Refined composition	$Ce_{0.95}Co_{2.59}Zn_{2.51}$	$Ce_{0.97}Ta_{0.06}Co_{4.28}Zn_{0.72}$
Formula mass	445.29	441.21
Space group, *Z*	*P*6/ ; 1	*P*6/ ; 1
(Å)	4.951(1)	5.108(1)
(Å)	4.065(1)	4.165(1)
$\mathcal{V}$ (Å^3)	86.29(4)	94.10(2)
d_c (Mg/m^3)	8.57	7.79
Radiation	Mo κ_α	Mo κ_α
reflns. collected/R_{int}	3706/0.053	1404/0.031
ind. data/restrains/params.	92/0/12	92/0/13
GoF (F^2)	1.194	1.130
R /*wR*2 [I $>2\sigma$(I)]	0.026/0.056	0.027/0.070
*R*1/*wR*2 [all data]	0.027/0.057	0.029/0.071
Largest diff peak/hole (/Å^3)	1.5/−0.9	2.2/−1.6

Table A.4
Atomic coordinates and equivalent isotropic displacement parameters ($Å^2 \times 10^3$) for Ta-free sample $Ce_{0.96}Co_{2.38}Zn_{2.65}$. *U* (*eq*) is defined as one third of the trace of the orthogonalized *Uij* tensor.

Element	Wyckoff Site	Occupancy	*x*	*y*	*z*	*U* (*eq*)
Ce	1a	0.95(1)	0	0	0	20(1)
Zn	2e	0.05(1)	0	0	0.305(7)	20(1)
Co	3g	0.55(9)	1/2	0	1/2	22(1)
Zn	3g	0.45(9)	1/2	0	1/2	22(1)
Co	2c	0.47(8)	2/3	1/3	0	13(1)
Zn	2c	0.53(8)	2/3	1/3	0	13(1)

Table A.5
Atomic coordinates and equivalent isotropic displacement parameters ($Å^2 \times 10^3$) for Ta-doped sample $Ce_{0.96}Ta_{0.04}Co_{4.35}Zn_{0.65}$. *U* (*eq*) is defined as one third of the trace of the orthogonalized *Uij* tensor.

Element	Wyckoff Site	Occupancy	*x*	*y*	*z*	*U* (*eq*)
Ce	1a	0.97(1)	0	0	0	15(1)
Ta	2e	0.03(1)	0	0	0.289(4)	15(1)
Co	3g	0.76(6)	1/2	0	1/2	9(1)
Zn	3g	0.24(6)	1/2	0	1/2	9(1)
Co	2c	1	2/3	1/3	0	18(1)

References

[1] J.M. Alameda, D. Givord, R. Lemaire, Q. Lu, Co energy and magnetization anisotropies in RCo5 intermetallics between 4.2 K and 300 K, J. Appl. Phys. 52 (3) (1981) 2079–2081, https://doi.org/10.1063/1.329622 arXiv: https://doi.org/10.1063/1.329622.

[2] K. Strnat, G. Hoffer, J. Olson, W. Ostertag, J.J. Becker, A family of new cobalt base permanent magnet materials, J. Appl. Phys. 38 (3) (1967) 1001–1002, https://doi.org/10.1063/1.1709459 arXiv: https://doi.org/10.1063/1.1709459.

[3] M. Bartashevich, T. Goto, R. Radwanski, A. Korolyov, Magnetic anisotropy and high-field magnetization process of CeCo5, J. Magn. Magn. Mater. 131 (1) (1994) 61–66, https://doi.org/10.1016/0304-8853(94)90010-8 URLhttp://www.sciencedirect.com/science/article/pii/0304885394900108.

[4] L. Nordström, O. Eriksson, M.S.S. Brooks, B. Johansson, Theory of ferromagnetism in $CeCo_5$, Phys. Rev. B 41 (1990) 9111–9120, https://doi.org/10.1103/physrevb.41.9111 URLhttps://link.aps.org/doi/10.1103/PhysRevB.41.9111.

[5] O. Makaryk, G. Dmytriv, D. Kevorkov, V. Pavlyuk, Comparison of the interaction of components in the La-Co-Zn and Ce-Co-Zn ternary systems at 470 K, J. Alloys Compd. 317–318 (2001) 448–449, https://doi.org/10.1016/s0925-8388(00)01367-0 the 13th International Conference on Solid Compounds of Transition Elements.http://www.sciencedirect.com/science/article/pii/S0925838800013670.

[6] V.P.O.Y. Zelinska, A.V. Zelinskii, X-ray Investigation of the RCo5–RZn5 (R= La, Ce, Sm, Gd, Tb) Quasibinary Systems, Visnyk of the Lviv University, 2011, pp. 41–47.

[7] Z. Malik, A. Grytsiv, P. Rogl, G. Giester, Phase relations and crystal structures in the system Ce-Ni-Zn at 800 C, J. Solid State Chem. 194 (2012) 80–90, https://doi.org/10.1002/chin.201247012 URLhttp://www.sciencedirect.com/science/article/pii/S0022459612004665.

[8] H. Okamoto, Ce-Co phase diagram, in: P. Villars, H. Okamoto, K. Cenzual (Eds.), ASM Alloy Phase Diagrams Database, section ed., ASM International, Materials Park, OH, 2006.

[9] P.C. Canfield, Z. Fisk, Growth of single crystals from metallic fluxes, Philos. Mag. 65 (6) (1992) 1117–1123, https://doi.org/10.1080/13642819208215073 arXiv: https://doi.org/10.1080/13642819208215073.

[10] P.C. Canfield, Solution Growth of Intermetallic Single Crystals: A Beginner's Guide, Properties and Appl ications of Complex Intermetallics, World Scientific, Singapore, 2010, https://doi.org/10.1142/9789814261647_0002 93–111.

[11] P.C. Canfield, I.R. Fisher, High-temperature solution growth of intermetallic single crystals and quasicrystals, J. Cryst. Growth 225 (2) (2001) 155–161, https://doi.org/article/pii/S0022024801008272.

[12] T.N. Lamichhane, M.T. Onyszczak, O. Palasyuk, S. Sharikadze, T.-H. Kim, M.J. Kramer, R.W. McCallum, A.L. Wysocki, M.C. Nguyen, V.P. Antropov, T. Pandey, D. Parker, S.L. Bud'ko, P.C. Canfield, A. Palasyuk, Single-crystal permanent magnets: extraordinary magnetic behavior in the Ta-, Cu-, and Fe-substituted CeCo5 systems, Phys. Rev. Appl. 11 (2018) 014052, https://doi.org/10.1103/PhysRevApplied. 11.014052.

[13] J. Rodríguez-Carvajal, Recent advances in magnetic structure determination by neutron powder diffraction, Physica B 192 (1–2) (1993) 55–69, https://doi.org/10.1016/0921-4526(93)90108-i.

[14] SMART (Bruker AXS Inc., Madison, Wisconsin, 1996).

[15] Wisconsin, 2000).

[16] SHELXTL (Bruker AXS Inc., Madison, for absorption anisotropy, Acta Crystallogr.

[17] R.H. Blessing, An empirical correction Section A 51 (1) (1995) 33–38, https://doi.org/10.1107/S0108767394005726.

Z. Malik, O. Sologub, G. Giester, P. Rogl, The system Ce-Zn-B at 800 C, J. Solid State Chem. 184 (11) (2011) 2840–2848, https://doi.org/10.1002/chin.201204008

URLhttp://www.sciencedirect.com/science/article/pii/S0022459611004609.

[18] V. Gorbunov, L. Grunau, N. Potapov, Structure of cobalt-rare earth alloys near the composition RCo5, Phys. Met. Metall. 37 (1) (1974) 105–109.

[19] A. Arrott, J.E. Noakes, Approximate equation of state for nickel near its critical temperature, Phys. Rev. Lett. 19 (14) (1967) 786–789, https://doi.org/10.1103/PhysRevLett. 19.786.

[20] A. Bhattachatyya, V. Deepti Jain, S. Ganesan, S. Majumbar Giri, Investigation of weak itinerant ferromagnetism and critical behavior of Y2Ni7, Phys. Rev. B 84 (2011) 184414, https://doi.org/10.1103/PhysRevB.84.184414.

[21] H.E. Stanley, Introduction to Phase Transitions and Critical Phenomena, Oxford University Press, 1987.

[22] W. Sucksmith, J.E. Thompson, The magnetic anisotropy of cobalt, Proc. R. Soc. London A: Math. Phys. Eng. Sci. 225 (1162) (1954) 362–375, https://doi.org/10.1098/rspa.1954.0209 URLhttp://rspa.royalsocietypublishing.org/content/225/1162/362.

[23] V. Taufour, S. Thimmaiah, S. March, S. Saunders, K. Sun, T.N. Lamichhane, M.J. Kramer, S.L. Bud'ko, P.C. Canfield, Structural and ferromagnetic properties of an orthorhombic phase of MnBi stabilized with Rh additions, Phys. Rev. Appl. 4 (2015) 014021, https://doi.org/10.1103/PhysRevApplied. 4.014021 URLhttp://link.aps.org/doi/10.1103/PhysRevApplied.4.014021.

org/10.1016/s0022-0248(01)00827-2 proceedings of the 12th American Conference on Crystal Growth and Epitaxy.http://www.sciencedirect.com/science/

[24] T.N. Lamichhane, V. Taufour, A. Palasyuk, Q. Lin, S.L. Bud'ko, P.C. Canfield, Ce3-xMgxCo9: transformation of a pauli paramagnet into a strong permanent magnet, Phys. Rev. Appl. 9 (2018) 024023, https://doi.org/10.1103/physrevapplied.9.024023.